# Shrinking instability of toroidal droplets

Alexandros A. Fragkopoulos, *Georgia Institute of Technology*
Ekapop Pairam, *King Mongkut's Institute of Technology*
Eric Berger, *Georgia Institute of Technology*
Phil Segre, *Emory University*
Alberto Fernández-Nieves, *Georgia Institute of Technology*

---

**Journal Title:** Proceedings of the National Academy of Sciences
**Volume:** Volume 114, Number 11
**Publisher:** National Academy of Sciences | 2017-03-14, Pages 2871-2875
**Type of Work:** Article | Final Publisher PDF
**Publisher DOI:** 10.1073/pnas.1619073114
**Permanent URL:** https://pid.emory.edu/ark:/25593/s4x0v

---

Final published version: http://dx.doi.org/10.1073/pnas.1619073114

# Shrinking instability of toroidal droplets

Alexandros A. Fragkopoulos[a], Ekapop Pairam[b], Eric Berger[a], Phil N. Segre[c], and Alberto Fernández-Nieves[a,1]

[a]School of Physics, Georgia Institute of Technology, Atlanta, GA 30332-0430; [b]Department of Food Engineering, King Mongkut's Institute of Technology Ladkrabang, Bangkok 10520, Thailand; and [c]Oxford College, Emory University, Oxford, GA 30054

Edited by David A. Weitz, Harvard University, Cambridge, MA, and approved January 24, 2017 (received for review November 18, 2016)

**Toroidal droplets are inherently unstable due to surface tension. They can break up, similar to cylindrical jets, but also exhibit a shrinking instability, which is inherent to the toroidal shape. We investigate the evolution of shrinking toroidal droplets using particle image velocimetry. We obtain the flow field inside the droplets and show that as the torus evolves, its cross-section significantly deviates from circular. We then use the experimentally obtained velocities at the torus interface to theoretically reconstruct the internal flow field. Our calculation correctly describes the experimental results and elucidates the role of those modes that, among the many possible ones, are required to capture all of the relevant experimental features.**

liquid tori | PIV | hydrodynamic instabilities | Stokes flow | stream function

The impact of drops with superhydrophobic surfaces (1), the corona splash that results after a drop hits a liquid bath (2), and the behavior of falling rain drops (3) all involve formation of transient toroidal droplets. These types of droplets have also been generated and studied via the Leidenfrost mechanism (4). Quite generally, a nonspherical droplet that is shaped as a torus is unstable and transforms into spherical droplets (5–8). For thin tori, this transformation happens via the Rayleigh–Plateau instability (Movie S1). In contrast, for thick-enough tori, there is no breakup and the toroidal droplet "shrinks" until it collapses onto itself to form a single spherical droplet (Movie S2). In the process, the tube radius grows until, eventually, the handle* of the torus disappears. Note that the spherical shape minimizes the surface area for a given volume. Hence, toroidal droplets always shrink to minimize surface area. The origin of this behavior can be understood from the variation of the mean curvature, $H$, and hence of the Laplace pressure, $\Delta p = 2\gamma H$, with $\gamma$ the interfacial tension, around the circular cross-section of the torus. Because $H$, and hence $\Delta p$, are larger on the outside of the torus than on its inside, the corresponding pressure difference causes the shrinking of the toroidal droplet (9). Assuming that the cross-section of the torus remains circular during the process and that the velocity at the interface is radial, in the reference frame of the circular cross-section, calculations of the shrinking speed were consistent with experimental observations (9). However, recent simulations have found that the cross-section does not remain circular but that it rather deforms significantly as the torus shrinks (10). Despite this difference with the theory, which brings about other additional differences in the flow fields, the simulated shrinking speed was also consistent with the experimental results. Overall, the underlying assumptions of the theory and the discrepancies with the simulation reflect that the shrinking instability of toroidal droplets is still not fully understood.

In this paper, we experimentally determine the flow field inside shrinking toroidal drops. We find that the droplet changes shape as it shrinks and that the velocity at the interface is not radial but rather has a significant tangential component. As a result, the flow field exhibits a characteristic circulation that helps to explain the observed shape. By considering the measured velocities at the droplet boundary, we theoretically obtain the velocity field inside the torus and highlight the relevance of the modes, among the many possible ones, required to capture the experimental features. Our experiments thus allow a complete description of the shrinking behavior of toroidal drops in the Stokes regime.

## Experimental Preliminaries

To determine the flow field, we use particle image velocimetry (PIV). We introduce optical heterogeneities in the liquid by adding tracer particles; these are polystyrene beads with an average diameter of 16.2 $\mu$m and a density of 1.06 g/mL. The method relies on video recording the time evolution of the liquid and spatially correlating the optical heterogeneities between consecutive frames, which allows assigning instantaneous velocities to different regions within an image. We use existent software [PIVLab (11)] and confirm the accuracy of the experimental setup and computer programs by video recording the motion of water with tracer particles rotating at a constant angular speed. We image along the rotation axis and confirm that the measured angular speed agrees with that imposed in the experiment.

To further test the experimental setup and data analysis, we perform experiments with sinking spherical droplets. In this case, the expected flow field is well known for any inner and outer liquid viscosities (13–15). We note that we choose the radius of these droplets so that they match the typical tube radius of our toroidal droplets. Because the liquid–liquid interface in our experiments is curved, light refraction could be significant, depending on the optical contrast between the liquids. Hence, these experiments also allow testing whether these effects play a dominant role in our experiments with toroidal droplets. The outer liquid is 1,000 centistokes (cSt) silicone oil, whereas the spherical droplets are made of deionized water with tracer particles. Because the respective densities are $\rho_o \approx 0.97$ g/mL and $\rho_i \approx 0.99$ g/mL, the droplets sink. We visualize the flow by illuminating with a laser sheet through the center of the droplet, as shown in Fig. 1*A*, and find that the flow has the typical

PHYSICS

### Significance

Liquid doughnuts or tori exhibit an inherent instability consisting in the shrinking of their "hole." For sufficiently thick tori, this behavior is the only route for the torus to become spherical and thus minimize the area for a given volume. Of note, this shrinking instability is not completely understood. In this work, we experimentally determine the flow field of toroidal droplets as they shrink and account for our observations by solving the relevant equations of motion in toroidal coordinates. We find that four modes, out of the many possible ones, are needed to successfully account for all of the relevant features in the experiment. These results highlight the rich fluid mechanics that results in the presence of interfaces with nonconstant mean curvature.

Author contributions: A.A.F., E.P., E.B., P.N.S., and A.F.-N. designed research; A.A.F., E.P., E.B., P.N.S., and A.F.-N. performed research; A.A.F., E.P., E.B., P.N.S., and A.F.-N. analyzed data; and A.A.F. and A.F.-N. wrote the paper.

The authors declare no conflict of interest.

This article is a PNAS Direct Submission.

[1]To whom correspondence should be addressed. Email: alberto.fernandez@physics.gatech.edu.

This article contains supporting information online at www.pnas.org/lookup/suppl/doi:10.1073/pnas.1619073114/-/DCSupplemental.

*The genus of a compact boundaryless surface is equal to the number of handles. A sphere has no handles, whereas a torus or a cup of coffee has one handle. The handle of the torus is then a global, topological property of the surface.

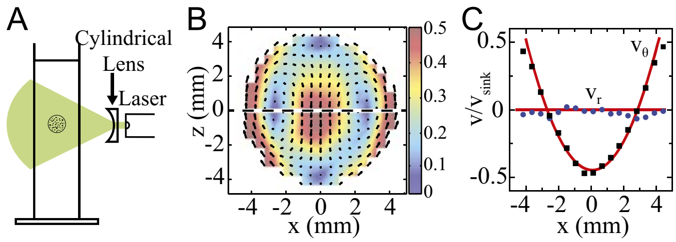


**Fig. 1.** (*A*) Schematic of the experimental setup for a sinking spherical droplet (not drawn to scale). The diameter of the drops we use is always equal or less than 8 mm, and they sink along the center of the cylindrical container, which has a diameter of 15 cm. (*B*) Averaged experimental flow field in the drop frame of reference. The color code corresponds to the speed normalized with the sinking speed, $v_{sink}$. (*C*) Experimental $v_r$ (blue circles) and $v_\theta$ (black squares) along the dashed line highlighted in *B*, together with the theoretical expectations. Note $\theta$ is measured with respect to the *z* axis.

circulation profile in the reference frame of the drop, expected for these situations, as shown in Fig. 1*B*. We note that the color code corresponds to the measured speeds, normalized with the sinking speed, which we measure independently using the distance traveled by the drop in 10 s. Theoretically, the velocity field, for the case where $\mu_i << \mu_o$, with $\mu_i$ and $\mu_o$ the inner and outer liquid viscosities, is given by (15):

$$v_r = \frac{v_{sink}}{2} \cos\theta \left(1 - \frac{r^2}{a^2}\right) \quad \textbf{[1a]}$$

$$v_\theta = -\frac{v_{sink}}{2} \sin\theta \left(1 - \frac{2r^2}{a^2}\right), \quad \textbf{[1b]}$$

where $r$ and $\theta$ are the usual two spherical coordinates, $v_r$ and $v_\theta$ are the velocities along the associated directions, and $v_{sink}$ is the sinking speed of the droplet. Note that the velocity has azimuthal symmetry. To quantitatively compare the experimental result and the theoretical expectations, we consider $v_r$ and $v_\theta$ along the dashed line in Fig. 1*B*. Both experiments and theory agree with each other, as shown in Fig. 1*C*, confirming the robustness of our setup, experimental procedures, and data analysis.

## Shrinking Toroidal Droplets

We generate toroidal droplets with controllable central-circle radius, $R_0$, and tube radius, $a_0$, as defined in Fig. 2, by injecting an inner liquid through a tip into a rotating continuous phase (5). The inner liquid is a 0.1 wt% solution of PEG in water containing tracer particles at a volume of fraction of 0.001. The continuous phase is a 60,000 cSt silicone oil that rotates at a constant angular speed, $\omega$, as schematically shown in Fig. 3*A*. For sufficiently high $\omega$, the shear exerted by the outside liquid onto the liquid exiting the tip induces formation of a jet, which follows the imposed rotation and closes up into a torus (5). The presence of PEG lowers the interfacial tension from $\gamma = (40 \pm 2)$ mN/m to $\gamma = (26 \pm 2)$ mN/m, hence slowing down the subsequent dynamics to allow enough time for any flow field due to the generation process to dissipate. As for a sinking spherical droplet, the flow inside a shrinking torus has azimuthal symmetry. It is thus enough to image the flow in a 2D cross-section through the center of the torus, which we do by using a laser sheet, as also shown in Fig. 3*A*.

A typical snapshot of a toroidal droplet during the shrinking process is shown in Fig. 3*B* (also see Movie S3); this droplet has an aspect ratio of $R_0/a_0 \approx 1.2$, which is below the threshold where Rayleigh–Plateau modes can cause breakup. Hence, these droplets can only evolve via shrinking. From the image, we realize that the cross-section of the torus does not remain circular. Instead, we observe that the initial circular cross-section elongates vertically and is slightly flatter near the inside of the torus. This result is qualitatively similar to what was seen in computer simulations (10). We then use PIV to determine the flow field inside the torus. The result associated with the image shown in Fig. 3*B* is presented in Fig. 3*C*. Note the color scale corresponds to the measured speed divided by the shrinking speed, $v_{sh}$, which we obtain by averaging the $x$-component of the velocity through the whole cross-section of the torus. The lack of up–down symmetry in the velocity field indicates that the observed flow field is not purely shrinking but that it also reflects the sinking of the toroidal droplet due to the density mismatch of the inner and outer liquids.

To isolate the flow associated with shrinking, we recall that the Reynolds number in our experiments is $Re \sim \mathcal{O}\left(10^{-6}\right)$, implying that we are well within the Stokes regime, where

$$\mu \Delta \mathbf{u} = \nabla p, \quad \textbf{[2]}$$

with velocity $\mathbf{u}$ and pressure $p$. Because the governing equations in our problem are linear, we can use the superposition principle and think of the flow in Fig. 3*C* as the sum of the flow associated with sinking and the flow associated with shrinking. Interestingly, these flows have differentiating up–down symmetries. Consider sinking first. In this case, $v_x$ is antisymmetric under a $z \to -z$ operation $[v_x(z) = -v_x(-z)]$, whereas $v_z$ is symmetric under a $z \to -z$ operation $[v_z(z) = v_z(-z)]$, as clearly seen in the schematic in Fig. 4*A*, where, for the sake of simplicity, we illustrate the situation for a thin toroidal droplet; the up–down symmetry reflected here, however, is general and maintained irrespective of the aspect ratio of the torus. For a shrinking droplet, however, $v_x(z) = v_x(-z)$ and $v_z(z) = -v_z(-z)$, as clearly seen in the schematic in Fig. 4*B*, where again we illustrate the situation for a thin toroidal droplet. We then obtain the symmetric and antisymmetric components of each of the velocity components, $v_i^S = [v_i(z) + v_i(-z)]/2$ and $v_i^A = [v_i(z) - v_i(-z)]/2$, with $i = x, z$, and take the symmetric part of $v_x$ and the antisymmetric part of $v_z$ to obtain the flow field associated with shrinking. The result is shown in Fig. 3*D*. Note that the flow now has the expected up–down symmetry. In addition, we see that the velocity is higher near the inside of the torus, reflective of the shrinking process. By subtracting $v_{sh}$, we obtain the flow field in the drop frame, as shown in Fig. 3*E*. It is now evident that the flow field is not radial at the interface but, instead, that there are both radial and tangential components of the velocity, which, in turn, causes a circulation that results from the viscous shear stresses exerted at the interface. In this frame of reference, we also see that there is a source near the outer part of the torus, which results from volume conservation and implies that as the torus shrinks, the tube radius must increase.

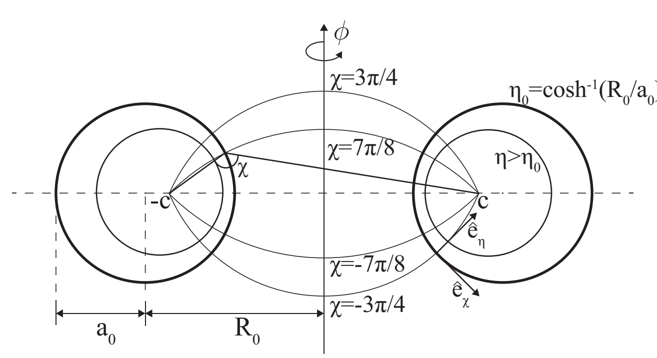


**Fig. 2.** Schematic of the cross-section of a torus illustrating the set of toroidal coordinates, $\eta$, $\chi$ and $\phi$, used in the calculations. The unit vectors, $\hat{e}_\eta$ and $\hat{e}_\chi$, as well as the central-circle radius, $R_0$, and the tube radius, $a_0$, are also shown.

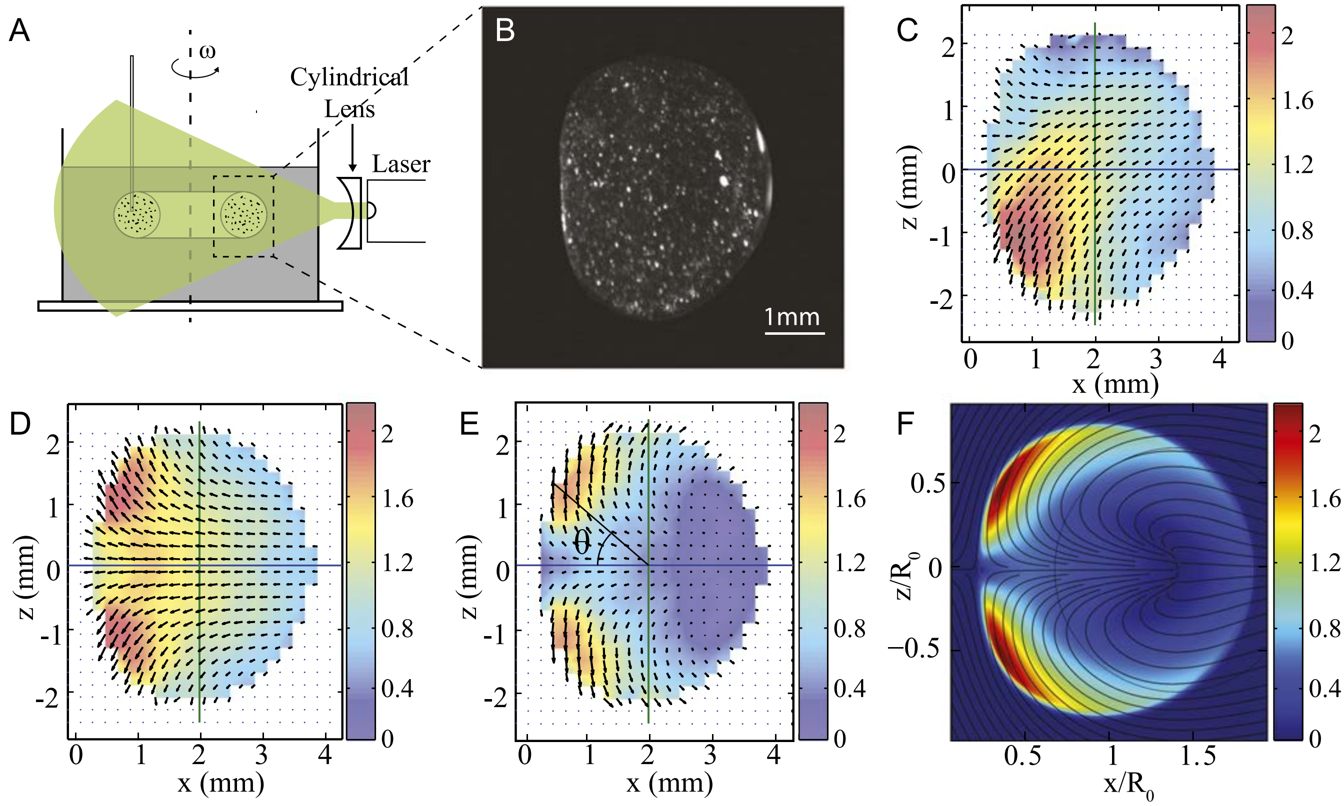


**Fig. 3.** (*A*) Schematic of the experimental setup for the generation of toroidal droplets together with the PIV setup (not drawn to scale). The cuvette is a parallelepiped with a square base of side 6 cm; the flat walls enable illuminating and imaging without refraction. Typical angular velocities are $\approx 2\pi$ rad/s. Typical injection flow rates are $\approx$50–60 mL/h. We note that as soon as the torus is formed, we remove the needle and stop the rotation. (*B*) Typical snapshot of a shrinking toroidal droplet with $R_0/a_0 \approx 1.2$. (*C*) Flow field obtained using PIV. (*D* and *E*) Flow field associated with shrinking in the laboratory frame (*D*) and in the drop frame (*E*). (*F*) Computer simulation of shrinking toroidal droplets in the drop frame. The color scales in *C*–*F* correspond to the measured speed normalized with $v_{sh}$.

To test the flow decomposition used to isolate the shrinking component, we perform computer simulations. We use the level set method for two phase flows in COMSOL Multiphysics (16) and simulate the experimental situation in the absence of gravity. We find that the overall drop deformation and flow field agrees well with our experimental findings, as shown in Fig. 3*F*. Also note that the flow field obtained in the simulations exhibits the up–down symmetries expected for shrinking. This result confirms the procedure to isolate the shrinking flow from the experimental flow field.

We then theoretically address the shrinking problem to understand the origin of the various features associated with the shrinking flow. We use the solution for the stream function, $\Psi$, in the Stokes regime in the set of toroidal coordinates ($\eta$, $\chi$, $\phi$) (9, 17). This coordinate system makes use of a focal circle with radius $c = \sqrt{R_0^2 - a_0^2} < R_0$. The coordinate $\phi$ is just the azimuthal angle. The coordinate $\chi$ is the angle defined with respect to the focal circle, as shown in Fig. 2; it can take values $\chi \in (-\pi, \pi]$. Finally, $\eta$, which is related to the aspect ratio of the torus, defines a given toroidal surface. Specifically, we take $\eta_0$ to be the value corresponding to our interface. As a result, $cosh\,(\eta_0) = R_0/a_0$. The inner part of the torus then corresponds to $\eta > \eta_0$, as shown in Fig. 2. In this coordinate system (9):

$$\Psi = \frac{c\, sinh\,(\eta)}{(cosh\,(\eta) - cos\,(\chi))^{3/2}} \sum_{n=-\infty}^{\infty} C_n\, sin(n\chi)\, Q^1_{n-3/2}(cosh(\eta)), \quad [3]$$

where $Q_l^m$ is the associated Legendre polynomial of the second kind, and $C_n$ are the amplitudes of each mode, which need to be determined. We make this determination by considering the experimental velocity at the interface and obtaining the radial, $v_r$, and tangential, $v_t$, components as a function of the polar angle $\theta$ (defined in Fig. 3*E*). We find that $v_r$ is not constant but that, instead, it peaks at $\theta \approx 50^o$ and $\theta \approx -50^o$, as shown by the blue line in Fig. 5*A* and consistent with the polar angle in the inside region of the torus below which the cross-section of the toroidal droplet is most deformed from the circular shape (Fig. 3*B*). Similarly, $v_t$ also has extrema at the same angle, as shown by the blue line in Fig. 5*B*.

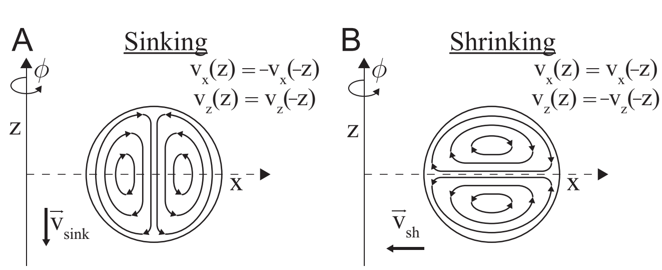


**Fig. 4.** Schematic illustrating the flow field in the drop frame inside a very thin toroidal droplet that either sinks (*A*) or shrinks (*B*). The up–down symmetries of the flow are highlighted at the top right of *A* and *B*.

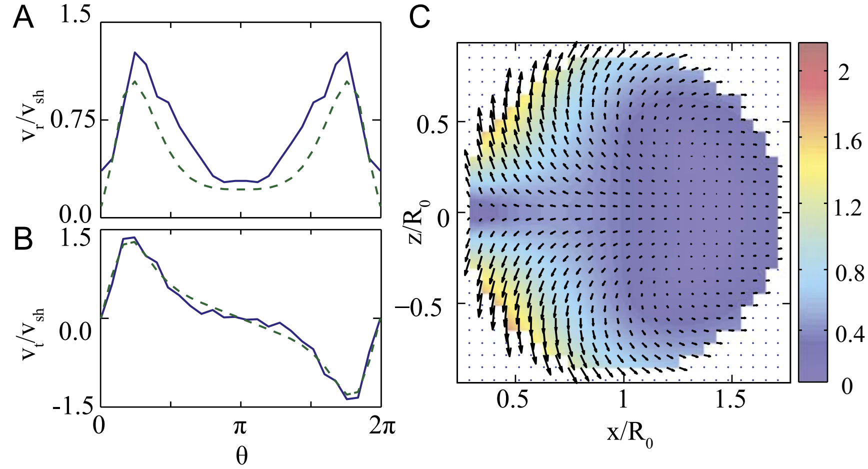


**Fig. 5.** (*A* and *B*) Radial, $v_r$ (*A*), and tangential, $v_t$ (*B*), velocities at the surface of the torus versus the polar angle $\theta$. Solid lines correspond to experiments, whereas dashed lines are theoretical fits. Note $\vec{v_r} = -v_r\hat{e_\eta}$ and $\vec{v_t} = -v_t\hat{e_\chi}$. (*C*) Flow field calculated from the stream function using the experimental boundary velocities. All velocities are scaled with $v_{sh}$.

From the stream function, we can calculate the velocity (18),

$$v_\eta = \frac{(cosh(\eta) - cos(\chi))^2}{c\ sinh(\eta)}\frac{\partial\Psi}{\partial\chi} \qquad \textbf{[4a]}$$

$$v_\chi = -\frac{(cosh(\eta) - cos(\chi))^2}{c\ sinh(\eta)}\frac{\partial\Psi}{\partial\eta}, \qquad \textbf{[4b]}$$

and use it to fit the experimental velocities at the interface to obtain the constants $C_n$. We find that by only considering the $n = -2, -1, 1, 2$ terms, we are able to capture all experimental features. Note that the $n = 0$ mode does not contribute because $\Psi = 0$ for $n = 0$. We emphasize that we perform a single simultaneous fit for both $v_r$ and $v_t$ while constraining the value of the constants $C_n$ by forcing the resultant velocity field to have the same shrinking speed as in the experiment. The result, shown in Fig. 5 *A* and *B* with dashed lines, correctly reproduces the experimental boundary velocities.

We obtain $C_{-2} = (0.2 \pm 0.1)v_{sh}$, $C_{-1} = (0.50 \pm 0.06)v_{sh}$, $C_1 = (-1.33 \pm 0.06)v_{sh}$, and $C_2 = (-0.4 \pm 0.1)v_{sh}$. Using these constants, we obtain the flow field inside the toroidal droplet. The result, shown in Fig. 5*C* in the drop frame, captures all relevant features seen in the experiments (Fig. 3*E*), including the circulation due to viscous stresses, the higher velocities in the inside region of the torus compared with those in the outside of the torus, and the presence of a source in the flow field near the outer part of the torus. We now consider each mode separately;

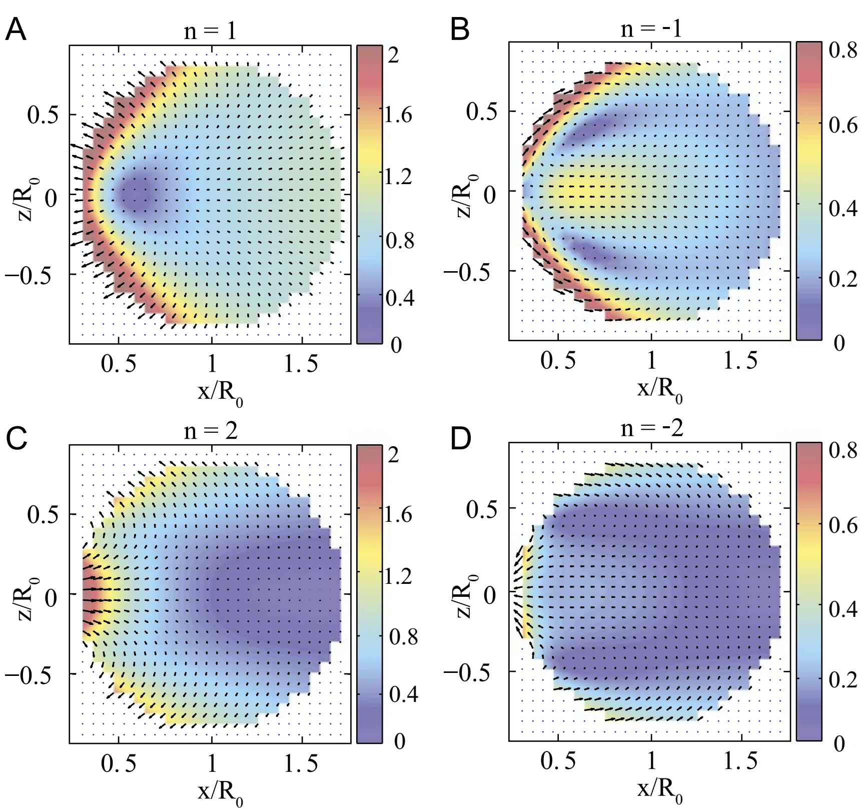


**Fig. 6.** $n = 1$ (*A*), $n = -1$ (*B*), $n = 2$ (*C*), and $n = -2$ (*D*) modes. The color code corresponds to the measured speeds normalized with $v_{sh}$.

these modes are shown in Fig. 6 in the drop frame. The $n = 1$ mode is radial at the interface, as shown in Fig. 6*A*, and has the largest weight of all four modes. This was the only mode considered in ref. 9 and is responsible for the increase in the tube radius as the torus shrinks. Note that in the presence of this mode only, the cross-section of the torus would remain approximately constant throughout the shrinking process. The $n = -1$ mode is tangential at the interface, as shown in Fig. 6*B*, and is responsible for the circulation seen experimentally. Finally, the $n = \pm 2$ modes can account for the shape we observe. The $n = 2$ mode produces a flow field that slows down the interface in the inside region of the torus, at $\theta \approx 0^o$, as shown in Fig. 6*C*, hence promoting the experimental flattening in this region. The $n = -2$ mode, shown in Fig. 6*D*, is very similar to the $n = 2$ mode, but with inverted velocities. Note the difference in the absolute values in the velocities, however, reflecting that the $n = 2$ mode dominates over the $n = -2$. Note also that the flow fields for each mode are all consistent with the expected up–down symmetries.

## Conclusions

We have experimentally obtained the flow field inside shrinking toroidal droplets using PIV and the linearity and symmetry properties of the flow in the problem. We observe that the cross-section of the torus does not remain circular over time but, rather, that it flattens in the inside region of the torus. Furthermore, the velocity at the interface has both radial and tangential components. We account for our observations by theoretically solving the Stokes equations using the stream function in toroidal coordinates. Four modes are enough to account for all experimental features. Of all modes, the $n = 1$ mode is the most significant and accounts for the flow field due to the expansion of the tube of the torus. The additional modes are needed to account for the observed circulation and deformation of the drop during shrinking. Overall, our results illustrate the behavior brought about by having interfaces with nonconstant mean curvature.

**ACKNOWLEDGMENTS.** We thank the National Science Foundation for financial support.

1. Renardy Y, et al. (2003) Pyramidal and toroidal water drops after impact on a solid surface. *J Fluid Mech* 484:69–83.
2. Yarin AL (2006) Drop impact dynamics: Splashing, spreading, receding, bouncing…. *Annu Rev Fluid Mech* 38:159–192.
3. Villermaux E, Bossa B (2009) Single-drop fragmentation determines size distribution of raindrops. *Nat Phys* 5(9):697–702.
4. Perrard S, Couder Y, Fort E, Limat L (2012) Leidenfrost levitated liquid tori. *Europhys Lett* 100(5):54006.
5. Pairam E, Fernández-Nieves A (2009) Generation and stability of toroidal droplets in a viscousliquid. *Phys Rev Lett* 102(23):234501.
6. Darbois Texier B, Piroird K, Quéré D, Clanet C (2013) Inertial collapse of liquid rings. *J Fluid Mech* 717:R3.
7. McGraw JD, Li J, Tran DL, Shi A-C, Dalnoki-Veress K (2010) Plateau-Rayleigh instability in a torus: Formation and breakup of a polymer ring. *Soft Matter* 6(6):1258–1262.
8. Mehrabian H, Feng JJ (2013) Capillary breakup of a liquid torus. *J Fluid Mech* 717:281–292.
9. Yao Z, Bowick MJ (2011) The shrinking instability of toroidal liquid droplets in the Stokes flow regime. *Eur Phys J E* 34(3):1–6.
10. Zabarankin M, Lavrenteva OM, Nir A (2015) Liquid toroidal drop in compressional Stokes flow. *J Fluid Mech* 785:372–400.
11. Thielicke W, Stamhuis EJ (2014) PIVlab—Time-resolved digital particle image velocimetry tool for MATLAB. Available at dx.doi.org/10.6084/m9.figshare.1092508. Accessed February 15, 2017.
12. Hadamard JSCR (1911) [Mouvement permanent lent d'une sphere liquide et visqueuse dans un liquide visqueux]. *CR Acad Sci* 152(25):1735–1738. French.
13. Batchelor GK (1967) *An Introduction to Fluid Dynamics* (Cambridge Univ Press, Cambridge, UK).
14. Levich VG (1962) Physicochemical Hydrodynamics (Prentice Hall, Englewood Cliffs, NJ).
15. Clift R, Grace JR, Weber ME (1978) *Bubbles, Drops, and Particles* (Academic, New York).
16. Sussman M, Smereka P, Osher S (1994) A level set approach for computing solutions to incompressible two-phase flow. *J Comput Phys* 114(1):146–159.
17. Khuri SA, Wazwaz AM (1997) On the solution of a partial differential equation arising in Stokes flow. *Appl Math Comput* 85(2):139–147.
18. Masoud H, Felske JD (2009) Analytical solution for Stokes flow inside an evaporating sessile drop: Spherical and cylindrical cap shapes. *Phys Fluids* 21(4):042102.